Facile Approach to Synthesize g-PAN/g-C$_3$N$_4$ Composites with Enhanced Photocatalytic H$_2$ Evolution Activity

Fang He, Gang Chen,* Yaoguang Yu, Sue Hao,* Yansong Zhou, and Yi Zheng

Department of Chemistry, Harbin Institute of Technology, Harbin 150001, P.R. China

Ⓢ *Supporting Information*

ABSTRACT: Novel composites consisting of graphitized polyacrylonitrile (g-PAN) nanosheets grown on layered g-C$_3$N$_4$ sheets were synthesized through a facile one-step thermal condensation of PAN and melamine for the first time. Photoluminescence spectroscopy and the photoelectrochemical measurements reveal that g-PAN nanosheets act as effective electron transfer channels to facilitate charge carrier separation in g-PAN/g-C$_3$N$_4$ composites. The g-PAN/g-C$_3$N$_4$ composites exhibit significantly enhanced visible-light photocatalytic performance for H$_2$ evolution over pristine g-C$_3$N$_4$. The 5.0 wt % g-PAN/g-C$_3$N$_4$ composite has optimal H$_2$ evolution rate of 37 μmol h^{-1}, exceeding 3.8 times over pristine g-C$_3$N$_4$. We have proposed a possible mechanism for charge separation and transfer in the g-PAN/g-C$_3$N$_4$ composites to explain the enhanced photocatalytic performance.

KEYWORDS: *graphitized polyacrylonitrile, graphitic carbon nitride, electron transfer channel, photocatalysis, H$_2$ evolution*
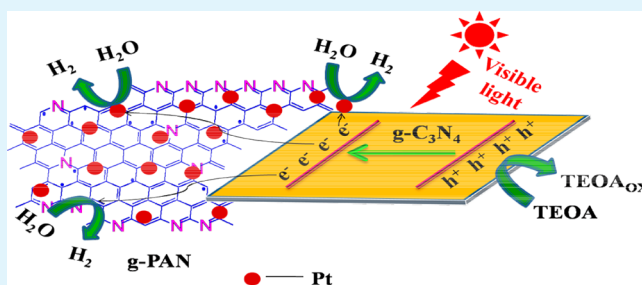
1. INTRODUCTION

Hydrogen is considered as a clean, renewable, and attractive energy source to substitute for fossil fuels. Since Fujishima and Honda reported photoelectrochemical water splitting in the TiO$_2$ electrode in 1972,[1] photocatalytic H$_2$ evolution from water by utilizing solar energy has received considerable attention because of its promising potential to solve the global energy and environmental problems.[2−5] Various semiconductor-based photocatalyst materials with visible-light responses have been explored for photocatalytic H$_2$ evolution, for instance, multicomponent oxides,[6,7] sulfides,[8] oxynitrides.[9] Moreover, polymeric materials including polyparaphenylene[10] have also shown photocatalytic H$_2$ evolution activity. Nevertheless, most of them can only respond to ultraviolet light with temperate activity. Therefore, development of high-efficiency polymeric photocatalysts with visible-light responses remains a challenge.

Recently, an organic and metal-free polymeric photocatalyst, graphitic carbon nitride (g-C$_3$N$_4$) with a proper band gap (2.7 eV) has attracted increasing attention. The g-C$_3$N$_4$ is proved to be photoactive for H$_2$ or O$_2$ evolution from water as well as photodegradation of pollutants in the visible-light region.[11−13] However, the efficiency for bulk g-C$_3$N$_4$ is far from satisfaction because of its low charge separation efficiency, poor absorption as well as low surface area. Extensive efforts have been devoted to enhancing the photocatalytic activity of g-C$_3$N$_4$, such as doping with metal/nonmetal elements,[14,15] protonation with HCl,[16] dye sensitizing,[17] construction of heterojunctions[18−20] and copolymerization.[21] Indubitably, the photocatalytic activity of g-C$_3$N$_4$ could be notably enhanced by introducing functional atoms or groups. Nevertheless, most of these modification methods need to be further improved for their potential disadvantages, such as tedious synthetic steps and introduction of metal and toxic solvents, which may increase the cost and pollute environment. Therefore, from the viewpoint of practical application, a relatively simple and easy synthesis approach to exploit efficient and environmentally friendly photocatalysts is of great importance.

Materials like polymer species with conjugated π electronic structures and visible-light absorption is nontoxic and can be the good candidate for the fast separation of photogenerated charge carriers.[22,23] It has been reported that the PANI-g-C$_3$N$_4$ composites show enhanced performance for MB photodegradation under visible-light illumination[24] and PPy-g-C$_3$N$_4$ composites exhibit remarkable enhanced photocatalytic H$_2$ evolution activity under simulated solar light illumination.[25] However, it should be noted that most of the polymer composites were generally obtained by tedious steps exhibiting aggregated morphologies. The polymer composite with a sheet-on-sheet morphology obtained by one-step method is rarely reported until now. Nanosheets possess a lot of advantage for photocatalysis such as large specific surface area offering more reactive sites and short diffusion distance decreasing the recombination rate of photogenerated charge carriers.[26] Among these materials, polyacrylonitrile (PAN) is an inexpensive polymeric material, which will form conjugated structures by heat treatment. When PAN is heated above 600 °C, it will lead to "graphitization". The graphitized PAN (g-
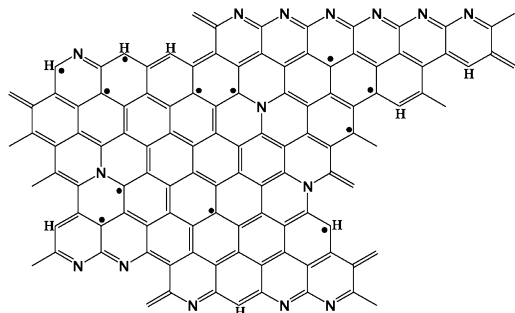
PAN) displays a layer sheet structure with graphite-like network structure (Scheme 1).

Scheme 1. Graphite-like Network Structure of g-PAN

The graphite-like network structure is beneficial for the fast charge transfer, which is worth anticipating that combing g-PAN nanosheets with layered g-C$_3$N$_4$ sheets will give excellent photocatalytic activity. Additionally, to the best of our knowledge, no prior study on the application of the g-PAN/g-C$_3$N$_4$ composite photocatalysts has been reported.

In this work, for the first time, g-PAN/g-C$_3$N$_4$ photocatalysts have been fabricated via a facile one-step synthesis by thermal condensation of melamine and PAN. The obtained g-PAN/g-C$_3$N$_4$ composites show significantly enhanced visible-light photocatalytic H$_2$ evolution performance over pristine g-C$_3$N$_4$. The effects of g-PAN contents on light absorption, surface areas, and efficiency of photocatalysis have been investigated in detail.

2. EXPERIMENTAL SECTION

2.1. Materials. Melamine (99%), triethanolamine (99%), and chloroplatinic acid hexahydrate were purchased from Sigma-Aldrich. Polyacrylonitrile was purchased from Shanghai MegaVision Membrane Engineering & Technology Co., Ltd. All chemicals were used without further purification.

2.2. Preparation of Photocatalysts. The pristine g-C$_3$N$_4$ or g-PAN obtained by simply heating melamine or PAN at 650 °C for 2 h under Ar gas flowing. The g-PAN/g-C$_3$N$_4$ composites were prepared as follows: First, melamine and PAN were mixed with a certain mass ratio and grinded in an agate mortar about 30 min. Then, the mixture was sintered under a gentle Ar flow at 650 °C for 2 h using an alumina boat. The mass ratios of PAN:melamine were 3, 5, 7, and 10 wt %, respectively.

2.3. Characterization. X-ray diffraction (XRD) measurements were recorded on a Rigaku D/max-2000 diffractometer using Cu Ka radiation ($\lambda = 0.15406$ nm). The morphologies of the photocatalysts were performed on a FEI, Tecnai G2 S-Twin TEM. Nitrogen adsorption−desorption isotherms were measured on an AUTOSORB-1-MP surface analyzer at 77 K. The UV−vis diffuse reflectance spectra (DRS) were measured on a TU-1900 spectrophotometer and the absorption spectra were obtained by the conversion of Kubelka−Munk approach, using BaSO$_4$ as the reflectance standard. Fourier transform infrared spectra were measured utilizing IR Affinity-1 FT-IR spectrometer. Raman measurement was carried out on a MODEL BX41TF Raman system using an excitation source of 532 nm Ar$^+$ laser. X-ray photoelectron spectroscopy (XPS) measurements were performed on an HI5700ESCA instrument with monochromatic Al Ka (1486.6 eV) X-ray radiation. The photoluminescence (PL) measurements were carried out at room temperature with a luminescence spectrometer (PerkinElmer, LS-55) using 375 nm as the excitation wavelength. Time-resolved fluorescence emission spectra were obtained on Edinburgh FLS 920 Fluorescence spectrometer.

2.4. Photoelectrochemical Measurements. Electrochemical measurements were performed on a CHI 660 C electrochemical instrument with a standard three-electrode system. The prepared electrodes act as working electrodes, using a Pt flake and Ag/AgCl (saturated KCl) as counter electrode and reference electrode, respectively. The light source utilizes a 300 W Xe arc lamp with a UV-cut off filter ($\lambda > 400$ nm). The electrolyte was Na$_2$SO$_4$ (0.5 mol L^{-1}) aqueous solution. Mott−Schottky plots were recorded at an AC voltage magnitude of 5 mV with the frequency of 100 Hz and at the potential range from −1.8 to 0 V. The photocurrent response was obtained at 0 V vs Ag/AgCl under visible light illumination. Electrochemical impedance spectroscopy (EIS) measurements were determined at an AC voltage magnitude of 5 mV with the frequency range of 10^5 to 10^{-1} Hz. Working electrodes were prepared as follows: FTO glass was washed sequentially with distilled water, ethanol and acetone in an ultrasonic cleaner for 30 min. Then, 0.05 g of g-C$_3$N$_4$ or 5 wt % g-PAN/g-C$_3$N$_4$ photocatalyst was ground with 1 mL of terpineol to obtain slurry, and then the slurry was coated onto 1 cm × 2 cm FTO glass electrode by the spin coater. After drying overnight in an oven, the electrodes were sintered at 350 °C for 1 h to improve adhesion.

2.5. Photocatalytic Reactions. The photocatalytic H$_2$ evolution reactions were carried out in a gas-closed circulation system with a side window. 0.1 g of photocatalyst was suspended in 300 mL of aqueous solution, containing 10 vol % triethanolamine (TEOA) as a sacrificial agent. 1.5 wt % Pt was loaded as cocatalyst by photodeposition of H$_2$PtCl$_6$·6H$_2$O. Before irradiation, suspensions were dispersed by sonication for 5 min and the reaction system was evacuated with N$_2$ for 25 min to remove oxygen. A 300 W Xe lamp was used as the light source with a cutoff filter ($\lambda > 400$ nm). The intensity of incident light was determined to be 20 mW cm^{-2} through a FZ-A radiometer. The evolved H$_2$ was measured by an online Agilent 7890 gas chromatography (TCD), using Ar as the carrier gas. Prior to use, all the glassware was cleaned with distilled water.
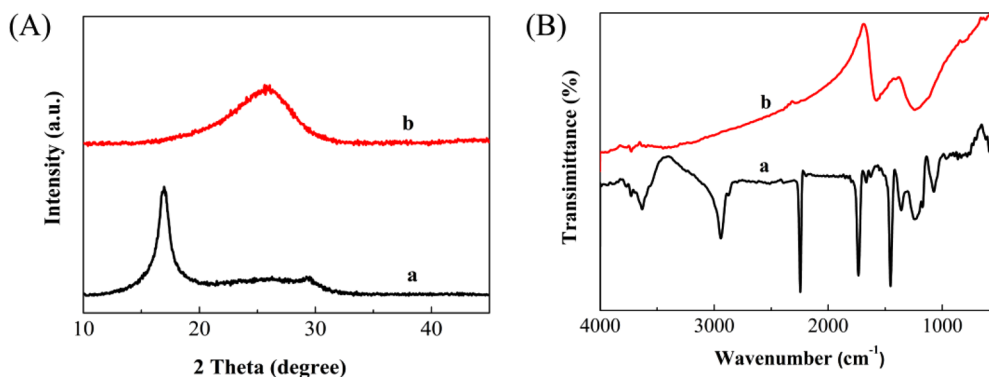

Figure 1. (A) XRD patterns and (B) FT-IR spectra of (a) PAN and (b) g-PAN, indicating that PAN has been graphitized to g-PAN.

3. RESULTS AND DISCUSSION

Figure 1A shows the XRD patterns of original PAN and g-PAN. The original PAN has a sharp intense peak at 17.5°, corresponding to the (100) diffraction of the hexagonal lattice. When PAN was heated in Ar flowing at 650 °C for 2 h, a broad diffraction peak appears at 26.0°, while the diffraction peak at 17.5° disappears, which is consistent with the literature,[27] indicating that PAN can be graphitized to g-PAN in the synthetic conditions. The chemical structures of g-PAN are further confirmed by FT-IR spectroscopy. Figure 1B displays the characteristic peaks of PAN at 2940 and 2240 cm^{-1} corresponding to stretch vibration of $-CH_2$ and $C\equiv N$, respectively, and 1452 cm^{-1} due to bend vibration of $-CH_2$. When PAN was heated at 650 °C, the characteristic peaks at 2940 and 2240 cm^{-1} disappear in the pyrolysis process because of the reaction of cyclization, elimination and aromatization.[28,29] Meanwhile, new peak appears at 1573 cm^{-1} due to stretch vibration of $C=C$ and $C=N$, whereas the peak at 1240 cm^{-1} is associated with C−N stretching mode and 805 cm^{-1} is assigned to aromatic heterocyclic ring, revealing that aromatic conjugated structure of g-PAN has formed during the graphitization progresses. The g-PAN with aromatic conjugated structure may act as an effective electron transfer channel leading to the fast photogenerated charge separation.

Figure 2 shows the Raman spectra of pristine g-C$_3$N$_4$, 5 wt % g-PAN/g-C$_3$N$_4$ composite and g-PAN. For g-PAN, the
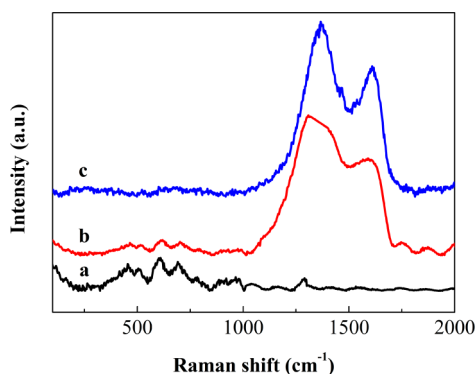
Figure 2. Raman spectra excited by 532 nm Ar$^+$ laser in air at room temperature of (a) g-C$_3$N$_4$, (b) 5 wt % g-PAN/g-C$_3$N$_4$ composite, and (c) g-PAN, which confirms that g-PAN exists in g-PAN/g-C$_3$N$_4$ composites.

characteristic peaks at 1603 and 1368 cm^{-1} are often referred as G-band and the D-band respectively for the graphitized structures.[30,31] The characteristic peaks of g-C$_3$N$_4$ shown in Figure 2 are in agreement with literature.[32] Moreover, all the Raman bands for g-C$_3$N$_4$ and g-PAN can be found in 5 wt % g-PAN/g-C$_3$N$_4$ composite, which confirms that g-PAN exists in g-PAN/g-C$_3$N$_4$ composites.

The morphologies of pristine g-C$_3$N$_4$ and 5 wt % g-PAN/g-C$_3$N$_4$ composite were investigated by TEM. As shown in Figure 3, pristine g-C$_3$N$_4$ displays big and smooth layer sheets. The 5 wt % g-PAN/g-C$_3$N$_4$ composite presents big layered sheets decorated with small flat nanosheets, which suggests that small g-PAN nanosheets grown on big layered g-C$_3$N$_4$ sheets to form layered g-PAN/g-C$_3$N$_4$ composites with intimate contacts. The junction can increase the contact area for fast interfacial charge transfer and shorten the time and distance for charge transfer,
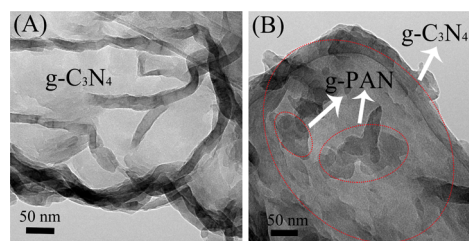
Figure 3. TEM images of (A) g-C$_3$N$_4$ and (B) 5 wt % g-PAN/g-C$_3$N$_4$ composite, which reveals small g-PAN nanosheets grown on big layered g-C$_3$N$_4$ sheets to form layered g-PAN/g-C$_3$N$_4$ composites.

which will promote the charge separation and thus enhance the photocatalytic activity.

The surface composition and binding state of the elements for 5 wt % g-PAN/g-C$_3$N$_4$ composite were studied by XPS. The XPS survey spectra in Figure 4A show that there are three elements of C, N and O in the composite. The high-resolution spectra of C and N elements in the 5 wt % g-PAN/g-C$_3$N$_4$ composite were further investigated. Figure 4B shows three distinct carbon species presented in the C 1s spectra. The peak at around 284.6 eV is regarded as graphitic carbon and carbon species from g-PAN[33] as well as g-C$_3$N$_4$,[34] whereas the peak at 286.3 eV is ascribed to C−NH$_2$ species on the g-C$_3$N$_4$.[35] The main C 1s peak at 288.0 eV corresponds to sp^2-hybridized carbon (N−C=N), which originates from g-PAN[33] and g-C$_3$N$_4$.[36] Figure 4 (C) shows three peaks detected in N 1s spectra. The main N 1s peak at 398.5 eV is assigned to sp^2-hybridized nitrogen (C=N−C), confirming the existence of graphite-like sp^2-bonded g-PAN[37] and g-C$_3$N$_4$.[34] Whereas the peak with binding energy of 400.1 eV originates from N−(C)$_3$ groups and the weakest peak at 401.1 eV is attributed to amino functions (C−N−H).

The BET specific surface areas and pore structures for pristine g-C$_3$N$_4$ and 5 wt % g-PAN/g-C$_3$N$_4$ composite were investigated by nitrogen adsorption−desorption. Figure 5 displays that the nitrogen adsorption−desorption isotherms for pristine g-C$_3$N$_4$ and 5 wt % g-PAN/g-C$_3$N$_4$ composite are type IV with H3 hysteresis loops, indicating the presence of mesopores.[38] As expected, 5 wt % g-PAN/g-C$_3$N$_4$ composite has larger specific surface areas (36 m^2 g^{-1}) than that of pristine g-C$_3$N$_4$ (22 m^2 g^{-1}). And the pore size distribution of 5 wt % g-PAN/g-C$_3$N$_4$ composite shows that it contains small mesopores of about 3.8 nm diameter. These data illustrate that g-PAN could introduce porous structure with increased surface area, which is favorable for enhancing the photocatalytic activity.

The optical absorption of pristine g-C$_3$N$_4$ and g-PAN/g-C$_3$N$_4$ composites with different PAN contents was measured using UV−vis DRS. It can be seen from Figure 6A that the absorption edge of pristine g-C$_3$N$_4$ is around 435 nm. Compared with pristine g-C$_3$N$_4$, g-PAN/g-C$_3$N$_4$ composites with the increase of g-PAN contents display strengthened and red-shift absorption, which is consistent with the color changes (from yellow to black). The band gaps for the composites are estimated by a classical Tauc approach.[39] As shown in Figure 6B, the band gaps of g-PAN/g-C$_3$N$_4$ composites range from 2.85 to 2.73 eV. Therefore, we can infer that the introduction of g-PAN is beneficial for the visible-light absorption of composites.

The band structure of g-PAN and g-C$_3$N$_4$ were investigated by VB XPS. As can be seen from Figure 7, the VB potentials for
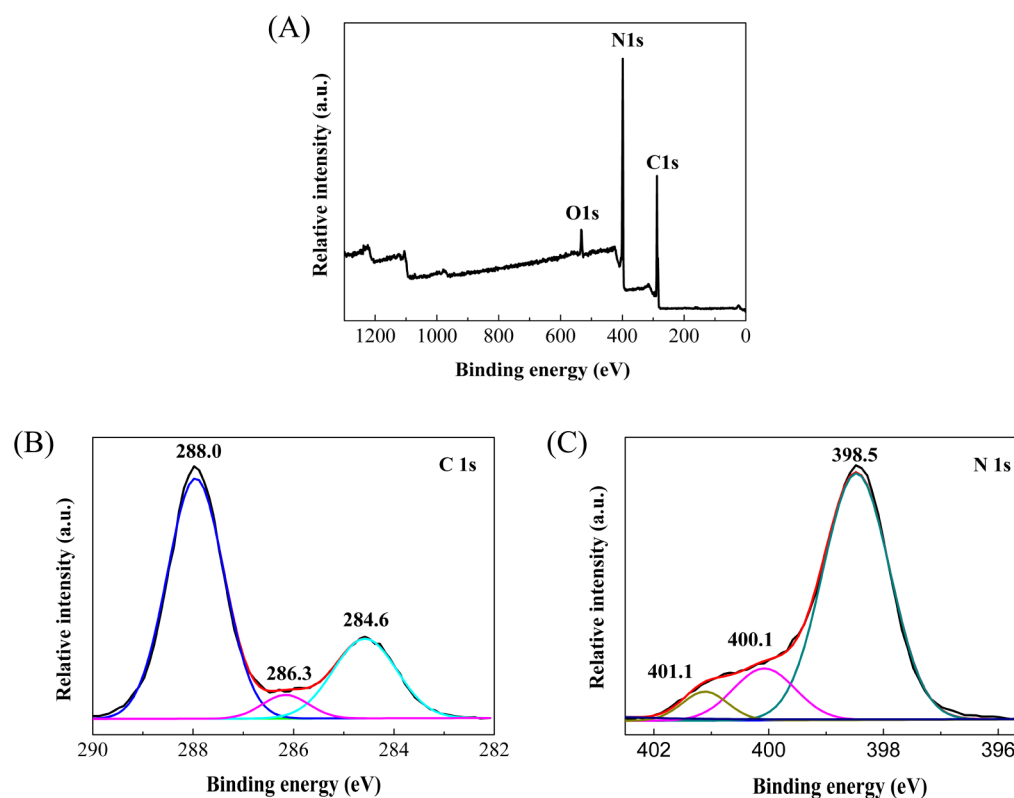
Figure 4. (A) XPS survey spectra, (B) high-resolution XPS spectra of C 1s, and (C) N 1s for 5 wt % g-PAN/g-C$_3$N$_4$ composite.
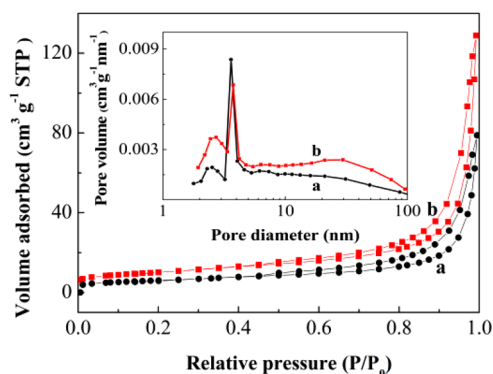

Figure 5. Nitrogen adsorption−desorption isotherms and the corresponding pore size distribution curves (inset) of (a) g-C$_3$N$_4$ and (b) 5 wt % g-PAN/g-C$_3$N$_4$ composite. The pore size distribution was determined from the desorption branch of the isotherm.

g-PAN and g-C$_3$N$_4$ are revealed to be 0.42 and 1.27 eV, respectively. The VB position for g-C$_3$N$_4$ is 0.85 V more positive than g-PAN. Combined with the energy gap, the CB position of g-C$_3$N$_4$ can be calculated to be −1.58 eV. This is consistent with the flat-band potential derived from Mott−Schottky plots (see Figure S1 in the Supporting Information). The flat-band potential for g-C$_3$N$_4$ is −0.5 V more negative over g-PAN, indicating the transfer of photogenerated electrons from g-C$_3$N$_4$ to g-PAN. Here, g-PAN sheets with conjugated structures function as an electron-transfer channel to fast transfer electrons to promote charge separation. On the basis of the relative VB and CB levels of g-PAN and g-C$_3$N$_4$, a schematic of the energy band alignment for g-PAN/g-C$_3$N$_4$ composites can be obtained (see Figure S2 in the Supporting

Information) to illustrate the separation and transfer of charge carriers at the interface between g-PAN and g-C$_3$N$_4$.

The photocatalytic performance for H$_2$ evolution of pristine g-C$_3$N$_4$ and g-PAN/g-C$_3$N$_4$ composites was evaluated with 1.5 Pt % in TEOA aqueous solution under visible-light illumination (λ > 400 nm). As shown in Figure 8A, the photocatalytic H$_2$ evolution rate of pristine g-C$_3$N$_4$ is 9.7 μmol h^{-1}. After introducing g-PAN, all g-PAN/g-C$_3$N$_4$ composites show higher H$_2$ evolution activity over pristine g-C$_3$N$_4$. The 5 wt % g-PAN/g-C$_3$N$_4$ composite has optimal H$_2$ evolution rate of 37 μmol h^{-1}, exceeding 3.8 times over pristine g-C$_3$N$_4$. That is due to the improved optical absorption, the larger surface area, and the fast photogenerated charge separation. When the g-PAN content is more than 5 wt %, the photocatalytic H$_2$ evolution will decrease with a further increase in g-PAN content. In consequence, a proper content of g-PAN is important for optimizing the photocatalytic activity of g-PAN/g-C$_3$N$_4$ composites. This decrease can be ascribed to the increase in a large black opacity g-PAN and light scattering, which will decrease the light going through the reaction suspension solution. Similar phenomena can be found in MWNTs/g-C$_3$N$_4$ composites[40] and α-Fe$_2$O$_3$ Nanorod/RGO composites.[41] Moreover, no obvious deactivation is detected for g-PAN/g-C$_3$N$_4$ composites after 6 h of continuous irradiation, illustrating that the sufficient stability of the composites for photocatalytic H$_2$ evolution.

The PL measurement for g-PAN/g-C$_3$N$_4$ composites with different PAN contents was performed to investigate the role of g-PAN in charge carrier separation. As shown in Figure 8B, the g-PAN/g-C$_3$N$_4$ composites give similar PL spectra to pristine g-C$_3$N$_4$. The PL emission intensity for the g-PAN/g-C$_3$N$_4$ composites decreases significantly with the increase in g-PAN contents, compared with pristine g-C$_3$N$_4$. This indicates that g-
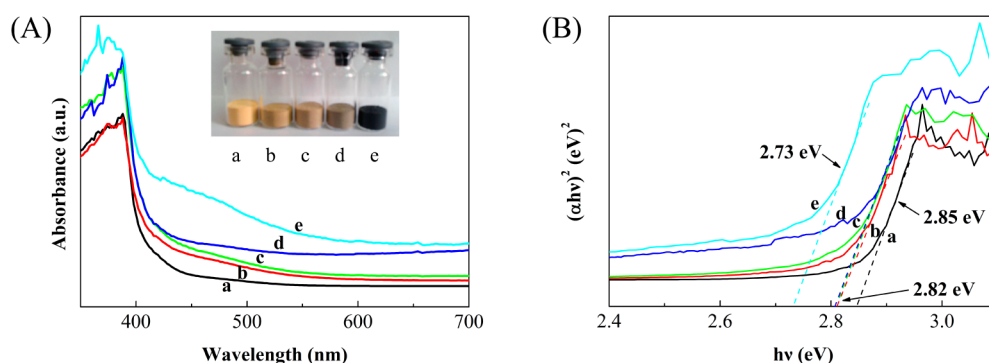
Figure 6. UV−vis absorption spectra converted from reflection to absorbance by the standard Kubelka−Munk method and the corresponding colors (inset) (A) and Plots of $(\alpha h\nu)^2$ vs photon energy ($h\nu$) for the band gap energy (B) of (a) g-C$_3$N$_4$, (b) 3 wt % g-PAN/g-C$_3$N$_4$, (c) 5 wt % g-PAN/g-C$_3$N$_4$, (d) 7 wt % g-PAN/g-C$_3$N$_4$, and (e) 10 wt % g-PAN/g-C$_3$N$_4$ composites.
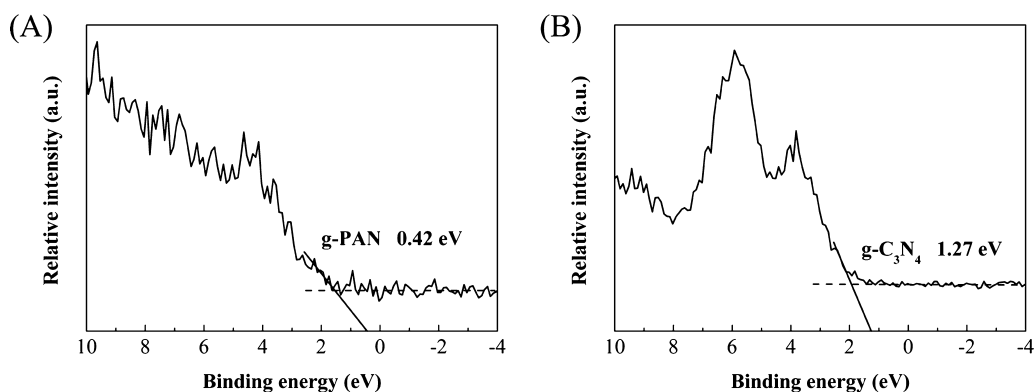
Figure 7. VB XPS spectra of (A) g-PAN and (B) g-C$_3$N$_4$, which suggests the VB position for g-C$_3$N$_4$ is 0.85 V more positive than g-PAN.
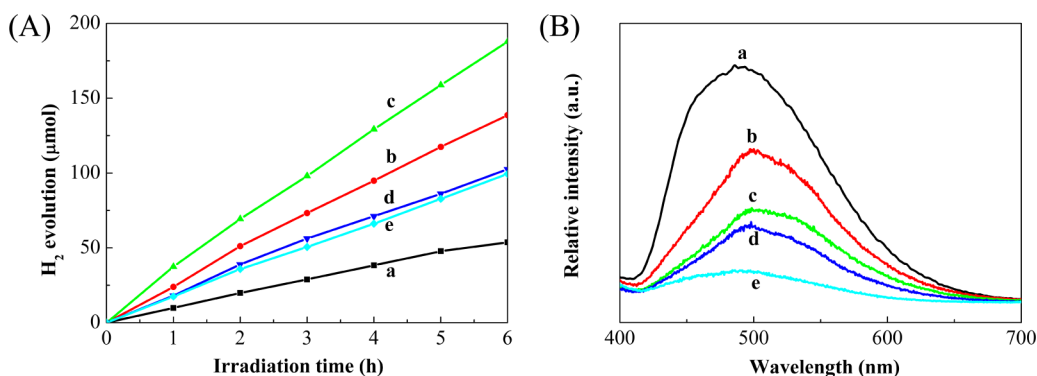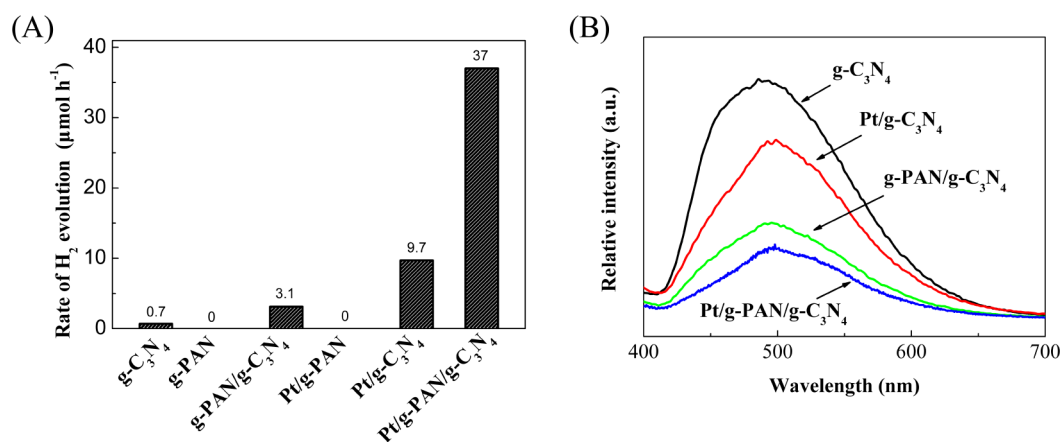

Figure 8. Photocatalytic H$_2$-evolution as a function of reaction time with 1.5 wt % Pt in 10 vol % TEOA aqueous solution under visible light irradiation (λ > 400 nm) (A) and Photoluminescence spectra under 375 nm excitation at room temperature (B) for (a) g-C$_3$N$_4$, (b) 3 wt % g-PAN/g-C$_3$N$_4$, (c) 5 wt % g-PAN/g-C$_3$N$_4$, (d) 7 wt % g-PAN/g-C$_3$N$_4$, and (e) 10 wt % g-PAN/g-C$_3$N$_4$ composites.

PAN/g-C$_3$N$_4$ composites have more efficient separation of photogenerated charge carriers under visible-light illumination, which is attributed to g-PAN with aromatic conjugated structures acting as effective electron transfer channel.

Figure 9A further confirms the role of g-PAN in improving the photocatalytic activity in g-PAN/g-C$_3$N$_4$ composites. As shown in Figure 9A, pristine g-C$_3$N$_4$ without adding Pt shows little photocatalytic activity because of the high recombination rate of photogenerated charge carriers. When g-PAN used as the photocatalyst even with Pt, no H$_2$ can be detected, which indicates that g-PAN is not active for photocatalytic H$_2$ evolution. However, after adding a little g-PAN, the photocatalytic H$_2$ evolution activity for 5 wt % g-PAN/g-C$_3$N$_4$

without adding Pt improves by 4.4 times, which confirms that g-PAN nanosheets can act as effective electron transfer channels as well as H$_2$ evolution sites. The photocatalytic activity of Pt/g-C$_3$N$_4$ for H$_2$ evolution improves almost 13.8 times. Furthermore, after introducing 5 wt % g-PAN to the Pt/g-C$_3$N$_4$, the photocatalytic H$_2$ evolution activity of Pt/5 wt % g-PAN/g-C$_3$N$_4$ increases by 52.8 times compared to that of pristine g-C$_3$N$_4$. This illustrates that g-PAN plays a crucial part in enhancing the photocatalytic H$_2$ evolution activity in the Pt/g-C$_3$N$_4$ composite system.

Figure 9B presents the PL spectra for pristine g-C$_3$N$_4$, Pt/g-C$_3$N$_4$, 5 wt % g-PAN/g-C$_3$N$_4$, and Pt/5 wt % g-PAN/g-C$_3$N$_4$. The PL intensity for Pt/g-C$_3$N$_4$ is a little bit lower than pristine

7175

dx.doi.org/10.1021/am500198y | ACS Appl. Mater. Interfaces 2014, 6, 7171−7179

Figure 9. (A) Comparison of the rate of photocatalytic H_2 evolution for g-C_3N_4, g-PAN, 5 wt % g-PAN/g-C_3N_4, Pt/g-PAN, Pt/g-C_3N_4, and Pt/5 wt % g-PAN/g-C_3N_4 in 10 vol % TEOA aqueous solution under visible light irradiation ($\lambda > 400$ nm). (B) Photoluminescence spectra for g-C_3N_4, Pt/g-C_3N_4, 5 wt % g-PAN/g-C_3N_4, and Pt/5 wt % g-PAN/g-C_3N_4 under 375 nm excitation at room temperature.

g-C_3N_4, but markedly higher than 5 wt % g-PAN/g-C_3N_4, which is in contrast to the varies of H_2 evolution activity, suggesting that Pt nanoparticles deposited on g-C_3N_4 mainly act as active sites and g-PAN plays more important part in charge separation. Furthermore, the PL intensity of Pt/5 wt % g-PAN/g-C_3N_4 is the lowest of all, illustrating that the synergistic effect among g-C_3N_4, g-PAN, and Pt improves photogenerated carrier separation leading to the optimum photocatalitic H_2 evolution.

The lifetime of the charge carriers for pristine g-C_3N_4 and 5 wt % g-PAN/g-C_3N_4 composite was further examined by the time-resolved fluorescence decay spectra. Figure 10 shows that
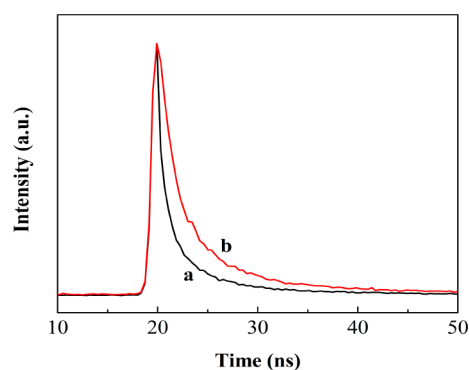
Figure 10. Time-resolved fluorescence decay spectra of (a) g-C_3N_4 and (b) 5 wt % g-PAN/g-C_3N_4 composite monitored at 500 nm excited by the 375 nm laser in air at room temperature by time-correlated single-photon counting.

the fluorescent intensities of pristine g-C_3N_4 and 5 wt % g-PAN/g-C_3N_4 composite decay exponentially. Fitting the decay spectra gives three radiative lifetimes with different percentages as listed in Table 1. The shortest lifetime and percentage of

Table 1. Radiative Fluorescence Lifetimes and Their Relative Percentages of Photoexcited Charge Carriers in the g-C_3N_4 and 5 wt % g-PAN/g-C_3N_4 Composite

| sample	τ_1(ns) (Rel %)	τ_2(ns) (Rel %)	τ_3(ns) (Rel %)
g-C_3N_4	0.92−24.22	3.93−47.74	18.53−28.04
5 wt % g-PAN/g-C_3N_4	1.26−24.49	4.45−49.49	17.66−26.02

charge carriers increase from 0.92 ns and 24.22% for pristine g-C_3N_4 to 1.26 ns and 24.49% for 5 wt % g-PAN/g-C_3N_4 composite. Both of the medium lifetime and percentage of charge carriers for pristine g-C_3N_4 and 5 wt % g-PAN/g-C_3N_4 composite increase from 3.93 ns and 47.74% to 4.45 ns and 49.49%, respectively. The lifetime for more than 70% of charge carriers has been effectively lengthened by compositing with a small amount of g-PAN on the g-C_3N_4 surface, which favors increasing the possibility of charge carriers participating in photocatalytic reactions.[26,42]

On the basis of the characterization results and the photocatalytic measurements for g-PAN/g-C_3N_4 composites, a possible photocatalytic H_2 evolution mechanism for g-PAN/g-C_3N_4 composites is proposed as shown in Figure 11. When g-
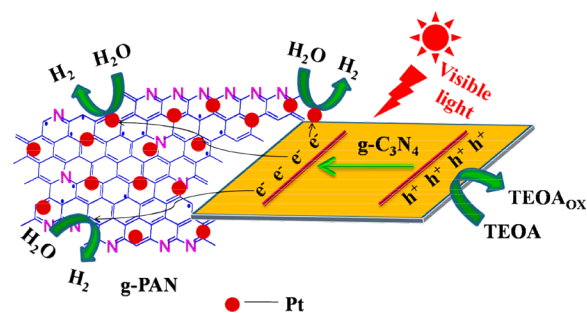
Figure 11. Schematic illustration for the enhanced photogenerated charge carriers separation and transfer in the g-PAN/g-C_3N_4 composites under visible light irradiation ($\lambda > 400$ nm).

C_3N_4 was irradiated with visible light, it will create electron−holes pairs. Generally, most of the charge carriers tend to rapidly recombine, and only a portion of charge carriers involve in the photocatalytic reaction, leading to low reactivity.[43] Nevertheless, when g-C_3N_4 modified by g-PAN, these photogenerated electrons of g-C_3N_4 tend to transfer to g-PAN sheets, leading to charge separation and effectively prolonging the charge carrier lifetime. Parts of the photogenerated electrons in the g-PAN nanosheets directly reduce water to H_2. In addition, the other electrons will transfer to the surface of Pt nanoparticles deposited on g-PAN nanosheets, and then reduce water to H_2. This indicates that the introduction of g-PAN nanosheets improves the interfacial charge transfer, which enhances the H_2 evolution. The holes at the VB of g-C_3N_4 can

7176

dx.doi.org/10.1021/am500198y | ACS Appl. Mater. Interfaces 2014, 6, 7171−7179
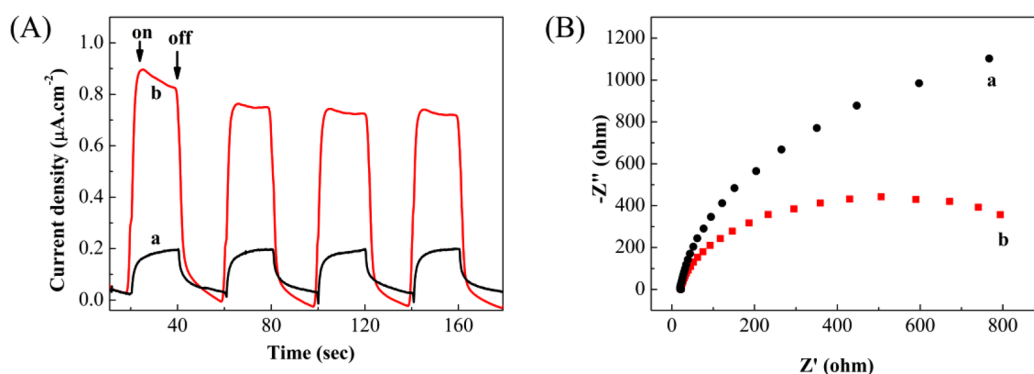
Figure 12. (A) Transient photocurrent recorded at 0 V bias vs Ag/AgCl and (B) EIS Nyquist plots obtained at an AC voltage with amplitude of 5 mV over the frequency range of 1×10^5 to 1×10^{-1} Hz for (a) g-C$_3$N$_4$ and (b) 5 wt % g-PAN/g-C$_3$N$_4$ electrodes in 0.5 mol L^{-1} Na$_2$SO$_4$ aqueous solution under visible light irradiation ($\lambda > 400$ nm).

react with TEOA. The possible photocatalytic reaction steps under visible-light illumination are proposed as follows

$$g\text{-}PAN/g\text{-}C_3N_4 \xrightarrow{hv} g\text{-}PAN(e^-)/g\text{-}C_3N_4(h^+) \tag{1}$$

$$g\text{-}PAN(e^-) + 2H^+ \rightarrow g\text{-}PAN + H_2 \tag{2}$$

$$g\text{-}PAN(e^-) + Pt \rightarrow g\text{-}PAN + Pt(e^-) \tag{3}$$

$$Pt(e^-) + 2H^+ \rightarrow Pt + H_2 \tag{4}$$

$$g\text{-}C_3N_4(h^+) + TEOA + OH^- \rightarrow TEOA_{ox} \tag{5}$$
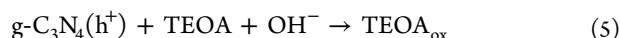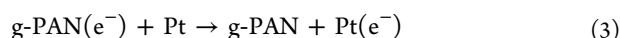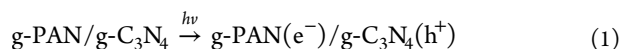
To verify the proposed photocatalytic mechanism, photocurrent responses were recorded. Figure 12A shows the photocurrent curve of g-C$_3$N$_4$ and 5 wt % g-PAN/g-C$_3$N$_4$ electrodes for several on−off cycles of irradiation. The value of photocurrent will quickly down to zero once the light turns off while the photocurrent will return to a steady value when the light turns on again, which is repeatable.[44,45] The 5 wt % g-PAN/g-C$_3$N$_4$ photoelectrode shows much higher photocurrent intensity over pristine g-C$_3$N$_4$, indicating that the g-PAN can efficiently suppress charge recombination by improving the interfacial charge transfer under visible light irradiation. The charge transfer resistance and separation efficiency have been investigated by electrochemical impedance spectroscopy (EIS).[46] Figure 12B reveals that the Nyquist plots diameter of 5 wt % g-PAN/g-C$_3$N$_4$ composite is much smaller over pristine g-C$_3$N$_4$, suggesting the lower resistance and the faster interfacial charge transfer. This is consistent with the photocurrent results. Overall, g-PAN nanosheets act as effective electron transfer channels in the g-PAN/g-C$_3$N$_4$ composites and promote the charge separation and thus obviously enhance the photocatalytic performance for H$_2$ evolution.

4. CONCLUSIONS

A facile one-step approach to synthesize sheet-on-sheet g-PAN/g-C$_3$N$_4$ composites has been developed for the first time. The obtained g-PAN/g-C$_3$N$_4$ composites show obviously enhanced photocatalytic H$_2$ evolution activity under visible light irradiation. The 5.0 wt % g-PAN/g-C$_3$N$_4$ composite has optimal H$_2$ evolution rate of 37 μmol h^{-1}, which exceeds 3.8 times that of pristine g-C$_3$N$_4$. It was shown that the g-PAN loading improves the optical absorption, surface area and the interfacial charge transfer as well as prolongs the charge carrier lifetime. A possible photocatalytic H$_2$ evolution mechanism is proposed. This work demonstrates that g-PAN can function as

an electron transfer channel for exploiting efficient photocatalytic materials applying in H$_2$ evolution and solar energy conversion. Meanwhile, this study provides new insights into a facile one-step thermal treatment approach to obtain composite materials modified by polymer species with promising potential applications.

■ ASSOCIATED CONTENT

Ⓢ Supporting Information
Mott−Schottky plots of g-PAN and g-C$_3$N$_4$ suggest that the derived flat-band potential for g-C$_3$N$_4$ is −0.5 V more negative than g-PAN; Band structure of g-PAN and g-C$_3$N$_4$ illustrates that the electrons transfer from the conduction band of g-C$_3$N$_4$ to the conduction band of g-PAN under visible light illumination. This material is available free of charge via the Internet at http://pubs.acs.org.

■ AUTHOR INFORMATION

Corresponding Author
*E-mail: gchen@hit.edu.cn. Tel/Fax: 0451-86413753.
Notes
The authors declare no competing financial interest.

■ ACKNOWLEDGMENTS

■ REFERENCES

(1) Fujishima, A.; Honda, K. Electrochemical Photolysis of Water at a Semiconductor Electrode. *Nature* **1972**, *238*, 37−38.
(2) Yu, Y. G.; Chen, G.; Wang, Q.; Li, Y. Hierarchical Architectures of Porous ZnS-Based Microspheres by Assembly of Heterostructure Nanoflakes: Lateral Oriented Attachment Mechanism and Enhanced Photocatalytic Activity. *Energy Environ. Sci.* **2011**, *4*, 3652−3660.
(3) Li, Y. X.; He, F.; Peng, S. Q.; Lu, G. X.; Li, S. B. Photocatalytic H$_2$ Evolution from NaCl Saltwater over ZnS$_{1−x−0.5y}$O$_x$(OH)$_y$−ZnO under Visible Light Irradiation. *Int. J. Hydrogen Energy* **2011**, *36*, 10565−10573.
(4) Sun, J. X.; Chen, G.; Wu, J. Z.; Dong, H. J.; Xiong, G. H. Bismuth Vanadate Hollow Spheres: Bubble Template Synthesis and Enhanced Photocatalytic Properties for Photodegradation. *Appl. Catal., B* **2013**, *132−133*, 304−314.
(5) Liu, M. C.; Wang, L. Z.; Lu, G. Q.; Yao, X. D.; Guo, L. J. Twins in Cd$_{1−x}$Zn$_x$S Solid Solution: Highly Efficient Photocatalyst for Hydrogen Generation from Water. *Energy Environ. Sci.* **2011**, *4*, 1372−1378.

(6) Liu, S. W.; Yu, J. G.; Jaroniec, M. Tunable Photocatalytic Selectivity of Hollow TiO_2 Microspheres Composed of Anatase Polyhedra with Exposed {001} Facets. *J. Am. Chem. Soc.* **2010**, *132*, 11914−11916.

(7) Yu, J. G.; Xiang, Q. J.; Zhou, M. H. Preparation, Characterization and Visible-Light-Driven Photocatalytic Activity of Fe-Doped Titania Nanorods and First-principles Study for Electronic Structures. *Appl. Catal., B* **2009**, *90*, 595−602.

(8) Li, Y. X.; Chen, G.; Wang, Q.; Wang, X.; Zhou, A. K.; Shen, Z. Y. Hierarchical $ZnS-In_2S_3-CuS$ Nanospheres with Nanoporous Structure: Facile Synthesis, Growth Mechanism, and Excellent Photocatalytic Activity. *Adv. Funct. Mater.* **2010**, *20*, 3390−3398.

(9) Aguiar, R.; Kalytta, A.; Reller, A.; Weidenkaff, A.; Ebbinghaus, S. G. Photocatalytic Decomposition of Acetone Using $LaTi(O,N)_3$ Nanoparticles under Visible Light Irradiation. *J. Mater. Chem.* **2008**, *18*, 4260−4265.

(10) Yanagida, S.; Kabumoto, A.; Mizumoto, K.; Pac, C.; Yoshino, K. Poly(Para-Phenylene)-Catalyzed Photoreduction of Water to Hydrogen. *J. Chem. Soc., Chem. Comm.* **1985**, *8*, 474−475.

(11) Wang, X. C.; Maeda, K.; Thomas, A.; Takanabe, K.; Xin, G.; Carlsson, J. M.; Domen, K.; Antonietti, M. A Metal-Free Polymeric Photocatalyst for Hydrogen Production from Water under Visible Light. *Nat. Mater.* **2009**, *8*, 76−80.

(12) Chu, S.; Wang, Y.; Guo, Y.; Feng, J.; Wang, C.; Luo, W.; Fan, X.; Zou, Z. Band Structure Engineering of Carbon Nitride: In Search of a Polymer Photocatalyst with High Photooxidation Property. *ACS Catal.* **2013**, *3*, 912−919.

(13) Martha, S.; Nashim, A.; Parida, K. M. Facile Synthesis of Highly Active g-C_3N_4 for Efficient Hydrogen Production under Visible Light. *J. Mater. Chem. A* **2013**, *1*, 7816−7824.

(14) Chen, X. F.; Zhang, J. S.; Fu, X. Z.; Antonietti, M.; Wang, X. C. Fe-g-C_3N_4-Catalyzed Oxidation of Benzene to Phenol Using Hydrogen Peroxide and Visible Light. *J. Am. Chem. Soc.* **2009**, *131*, 11658−11659.

(15) Liu, G.; Niu, P.; Sun, C.; Smith, S. C.; Chen, Z.; Lu, G. Q.; Cheng, H.-M. Unique Electronic Structure Induced High Photoreactivity of Sulfur-Doped Graphitic C_3N_4. *J. Am. Chem. Soc.* **2010**, *132*, 11642−11648.

(16) Zhang, Y. J.; Thomas, A.; Antonietti, M.; Wang, X. C. Activation of Carbon Nitride Solids by Protonation: Morphology Changes, Enhanced Ionic Conductivity, and Photoconduction Experiments. *J. Am. Chem. Soc.* **2009**, *131*, 50−51.

(17) Min, S. X.; Lu, G. X. Enhanced Electron Transfer from the Excited Eosin Y to mpg-C_3N_4 for Highly Efficient Hydrogen Evolution under 550 nm Irradiation. *J. Phys. Chem. C* **2012**, *116*, 19644−19652.

(18) Yan, S. C.; Lv, S. B.; Li, Z. S.; Zou, Z. G. Organic-Inorganic Composite Photocatalyst of g-C(3)N(4) and TaON with Improved Visible Light Photocatalytic Activities. *Dalton Trans.* **2010**, *39*, 1488−1491.

(19) Pan, C. S.; Xu, J.; Wang, Y. J.; Li, D.; Zhu, Y. F. Dramatic Activity of $C_3N_4/BiPO_4$ Photocatalyst with Core/Shell Structure Formed by Self-Assembly. *Adv. Funct. Mater.* **2012**, *22*, 1518−1524.

(20) Wang, Y. J.; Shi, R.; Lin, J.; Zhu, Y. F. Enhancement of Photocurrent and Photocatalytic Activity of ZnO Hybridized with Graphite-Like C_3N_4. *Energy Environ. Sci.* **2011**, *4*, 2922−2929.

(21) Zhang, J. S.; Chen, X. F.; Takanabe, K.; Maeda, K.; Domen, K.; Epping, J. D.; Fu, X.; Antonietti, M.; Wang, X. Synthesis of a Carbon Nitride Structure for Visible-Light Catalysis by Copolymerization. *Angew. Chem., Int. Ed.* **2010**, *49*, 441−444.

(22) Zhang, L. W.; Fu, H. B.; Zhu, Y. F. Efficient TiO_2 Photocatalysts from Surface Hybridization of TiO_2 Particles with Graphite-Like Carbon. *Adv. Funct. Mater.* **2008**, *18*, 2180−2189.

(23) Zhang, H.; Zong, R.; Zhu, Y. F. Photocorrosion Inhibition and Photoactivity Enhancement for Zinc Oxide via Hybridization with Monolayer Polyaniline. *J. Phys. Chem. C* **2009**, *113*, 4605−4611.

(24) Ge, L.; Han, C. C.; Liu, J. In Situ Synthesis and Enhanced Visible Light Photocatalytic Activities of Novel PANI−g-C_3N_4 Composite Photocatalysts. *J. Mater. Chem.* **2012**, *22*, 11843−11850.

(25) Sui, Y.; Liu, J. H.; Zhang, Y. W.; Tian, X. K.; Chen, W. Dispersed Conductive Polymer Nanoparticles on Graphitic Carbon Nitride for Enhanced Solar-Driven Hydrogen Evolution from Pure Water. *Nanoscale* **2013**, *5*, 9150−9155.

(26) Niu, P.; Zhang, L.; Liu, G.; Cheng, H. M. Graphene-Like Carbon Nitride Nanosheets for Improved Photocatalytic Activities. *Adv. Funct. Mater.* **2012**, *22*, 4763−4770.

(27) Ko, T. H.; Chen, C.Y. J. Raman Spectroscopic Study of the Microstructure of Carbon Films Developed from Cobalt Chloride-Modified Polyacrylonitrile. *Appl. Polym. Sci.* **1999**, *71*, 2219−2225.

(28) Setnescu, R.; Jipa, S.; Setnescu, T.; Kappel, W.; Kobayashi, S.; Osawa, Z. IR and X-ray Characterization of the Ferromagnetic Phase of Pyrolysed Polyacrylonitrile. *Carbon* **1999**, *37*, 1−6.

(29) Bojdys, M. J.; Muller, J. O.; Antonietti, M.; Thomas, A. Ionothermal Synthesis of Crystalline, Condensed, Graphitic Carbon Nitride. *Chem.—Eur. J.* **2008**, *14*, 8177−8182.

(30) Yao, Y.; Zhou, T.; Yang, T.; Xiang, R.; Wu, Y. Homogeneous Thermal Stabilization of Polyacrylonitrile in an Ionic Liquid Solution for the Production of Carbon Nanospheres. *Carbon* **2013**, *58*, 249−251.

(31) Gu, H. B.; Rapole, S. B.; Huang, Y. D.; Cao, D. M.; Luo, Z. P.; Wei, S. Y.; Guo, Z. H. Synergistic Interactions between Multi-Walled Carbon Nanotubes and Toxic Hexavalent Chromium. *J. Mater. Chem. A* **2013**, *1*, 2011−2021.

(32) Xiang, Q. J.; Yu, J. G.; Jaroniec, M. Preparation and Enhanced Visible-Light Photocatalytic H_2-Production Activity of Graphene/C_3N_4 Composites. *J. Phys. Chem. C* **2011**, *115*, 7355−7363.

(33) Pirlot, C.; Willems, I.; Fonseca, A.; Nagy, J. B.; Delhalle, J. Preparation and Characterization of Carbon Nanotube/Polyacrylonitrile Composites. *Adv. Eng. Mater.* **2002**, *4*, 109−114.

(34) Zhang, J. S.; Zhang, M. W.; Zhang, G. G.; Wang, X. C. Synthesis of Carbon Nitride Semiconductors in Sulfur Flux for Water Photoredox Catalysis. *ACS Catal.* **2012**, *2*, 940−948.

(35) Li, J. H.; Shen, B.; Hong, Z. H.; Lin, B. Z.; Gao, B. F.; Chen, Y. L. A Facile Approach to Synthesize Novel Oxygen-Doped g-C_3N_4 with Superior Visible-Light Photoreactivity. *Chem. Commun.* **2012**, *48*, 12017−12019.

(36) Thomas, A.; Fischer, A.; Goettmann, F.; Antonietti, M.; Müller, J. O.; Schlögl, R.; Carlsson, J. M. Graphitic Carbon Nitride Materials: Variation of Structure and Morphology and Their Use as Metal-Free Catalysts. *J. Mater. Chem.* **2008**, *18*, 4893−4908.

(37) Luo, Q. Z.; Li, X. Y.; Li, X. Y.; Wang, D. S.; An, J.; Li, X. X. Visible Light Photocatalytic Activity of TiO_2 Nanoparticles Modified by Pre-Oxidized Polyacrylonitrile. *Catal. Commun.* **2012**, *26*, 239−243.

(38) Yu, J. G.; Qi, L. F.; Jaroniec, M. Hydrogen Production by Photocatalytic Water Splitting over Pt/TiO_2 Nanosheets with Exposed (001) Facets. *J. Phys. Chem. C* **2010**, *114*, 13118−13125.

(39) Reddy, K. H.; Martha, S.; Parida, K. M. Fabrication of Novel p-BiOI/n-$ZnTiO_3$ Heterojunction for Degradation of Rhodamine 6G under Visible Light Irradiation. *Inorg. Chem.* **2013**, *52*, 6390−6401.

(40) Ge, L.; Han, C. C. Synthesis of MWNTs/g-C_3N_4 Composite Photocatalysts with Efficient Visible Light Photocatalytic Hydrogen Evolution Activity. *Appl. Catal., B* **2012**, *117–118*, 268−274.

(41) Pradhan, G. K.; Padhi, D. K.; Parida, K. M. Fabrication of α-Fe_2O_3 Nanorod/RGO Composite: A Novel Hybrid Photocatalyst for Phenol Degradation. *ACS Appl. Mater. Interfaces* **2013**, *5*, 9101−9110.

(42) Dong, F.; Zhao, Z. W.; Xiong, T.; Ni, Z. L.; Zhang, W. D.; Sun, Y. J.; Ho, W. K. In Situ Construction of g-C_3N_4/g-C_3N_4 Metal-Free Heterojunction for Enhanced Visible-Light Photocatalysis. *ACS Appl. Mater. Interfaces* **2013**, *5*, 11392−11401.

(43) Yu, J. G.; Wang, W. G.; Cheng, B.; Su, B. L. Enhancement of Photocatalytic Activity of Mesoporous TiO_2 Powders by Hydrothermal Surface Fluorination Treatment. *J. Phys. Chem. C* **2009**, *113*, 6743−6750.

(44) Bu, Y. Y.; Chen, Z. Y.; Li, W. B. Using Electrochemical Methods to Study the Promotion Mechanism of the Photoelectric Conversion Performance of Ag-Modified Mesoporous g-C_3N_4 Heterojunction Material. *Appl. Catal., B* **2014**, *144*, 622−630.

(45) Zhang, Y. J.; Mori, T.; Niu, L.; Ye, J. H. Non-Covalent Doping of Graphitic Carbon Nitride Polymer with Graphene: Controlled Electronic Structure and Enhanced Optoelectronic Conversion. *Energy Environ. Sci.* **2011**, *4*, 4517−4521.

(46) Yang, S.; Gong, Y.; Zhang, J.; Zhan, L.; Ma, L.; Fang, Z.; Vajtai, R.; Wang, X.; Ajayan, P. M. Exfoliated Graphitic Carbon Nitride Nanosheets as Efficient Catalysts for Hydrogen Evolution under Visible Light. *Adv. Mater.* **2013**, *25*, 2452−2456.